ORIGINAL ARTICLE

An overlooked aspect concerning the effect of the spatial pattern of zonal wind stress anomalies on El Niño evolution and diversity

Xianghui Fang[1,2,3] · Henk Dijkstra[4,5] · Claudia Wieners[4,5] · Francesco Guardamagna[4,5]

Abstract

Anomalous zonal wind stress in the central-to-western Pacific plays a crucial role in ENSO evolution by exciting oceanic waves that propagate eastward or westward. However, compared to its intensity, the importance of its spatial pattern is an overlooked aspect in ENSO theory. Using a linear regression model and numerical simulations with the Zebiak-Cane model, we here show that the zonal wind stress anomaly pattern significantly affects the development of El Niño and its type. Specifically, if the westerly wind stress is closer to the western Pacific (WP), the excited upwelling Rossby waves will take less time to reach the WP coast before they are reflected as Kelvin waves. This significantly weakens sea surface temperature anomalies in the eastern Pacific region since less time is provided for their amplification due to positive feedbacks. This causes the anomalous warming center to be closer to the central Pacific (CP) region, leading to a CP-type El Niño.

1 Introduction

Although El Niño-Southern Oscillation (ENSO) occurs and develops in the tropical Pacific, its influence on climate and weather can reach many regions of the world (Philander 1983; Ropelewski and Halpert 1987; Klein et al. 1999; McPhaden et al. 2006; Zhang et al. 2017). Therefore, understanding the physical mechanism of ENSO and effectively predicting it has always been an important topic in climate science. The classical delayed oscillator theory (Battisti 1988; Schopf and Suarez 1988) suggests that the anomalous westerly wind stress in the equatorial central Pacific (CP) can excite a downwelling Kelvin wave (warming signal on the equator), which propagates eastward rapidly (~ 2.5 m/s). When it arrives at the eastern Pacific (EP), where the mean thermocline is quite shallow, the wave can effectively warm the local sea surface temperature (SST) through upwelling. The induced anomalous warming in the EP weakens the temperature gradient between the western Pacific (WP) and the EP, and thus the Walker circulation, which further strengthens the anomalous westerly wind stress in the CP. This positive feedback is called the thermocline feedback (Bjerknes 1969), and is considered as the dominant mechanism for ENSO development. On the other hand, the anomalous westerly wind stress also stimulates upwelling Rossby waves (cold signal) on both sides off the equator. These waves propagate westward much slower as the speed of the fastest Rossby wave is only 1/3 of that of the Kelvin wave. When reaching the western boundary, they are effectively reflected as upwelling Kelvin waves at the equator. Since these reflected waves raise the thermocline, they will suppress and terminate anomalous warming in the EP region. Thus, the time interval between the excited and reflected Kelvin waves is crucial for the SST development in the EP region.

The delayed oscillator theory is a great contribution for understanding the ENSO phenomenon and has guided many modeling works (Tang et al. 2018; Wang 2018). It clearly stresses the importance of anomalous zonal wind stress in

✉ Xianghui Fang
fangxh@fudan.edu.cn

1 Department of Atmospheric and Oceanic Sciences, Institute of Atmospheric Sciences, Fudan University, Shanghai, China

2 Shanghai Key Laboratory of Ocean-Land-Atmosphere Boundary Dynamics and Climate Change, Fudan University, Shanghai, China

3 Shanghai Frontiers Science Center of Atmosphere-Ocean Interaction, Shanghai, China

4 Institute for Marine and Atmospheric research Utrecht, Utrecht University, Utrecht, The Netherlands

5 Centre for Complex Systems Studies, Utrecht University, Utrecht, The Netherlands

the equatorial CP region on subsequent ENSO evolution and thus makes this variable an important predictor for ENSO forecasting models (Clarke and van Gorder 2001; Ruiz et al. 2005; Ren et al. 2019; Fang and Zheng 2021). Besides, the thermocline depth (TCD) is also critical in this theory. In subsequent theoretical work, Jin (1997) further emphasized the importance of the exchange of warm water volume (or the zonal mean TCD anomalies (TCDa) between the equatorial and off-equatorial Pacific on the development and decay of ENSO, i.e., the recharge oscillator theory. This was well verified by further observational studies (Meinen and McPhaden 2000; McPhaden 2003). Therefore, the zonal mean TCDa of the equatorial Pacific is another important predictor in ENSO forecasting (Clarke and van Gorder 2001; Fang and Mu 2018a).

Note that these classical theories were mainly built to understand the canonical EP type ENSO, and they cannot accurately describe the later identified CP type (Kug et al. 2009; Capotondi et al. 2015; Timmermann et al. 2018). In fact, studies have shown that due to the CP region being bordered by the warm pool to the west and the cold tongue to the east, the zonal gradient of the mean SST is relatively strong, which makes the zonal advective feedback play a crucial role in the SST variation here (Kug et al. 2009; Fang and Mu 2018b; Pang et al. 2023; Fang et al. 2024). However, under a specific background mean state, the question remains why different types of ENSO appear. Many recent studies emphasize the importance of atmospheric or oceanic stochasticity in characterizing the complexity of ENSO (Geng et al. 2020; Geng and Jin 2022, 2023; Chen et al. 2022; Chen and Fang 2023; Fang and Chen 2023;), but new analysis of deterministic models may provide relevant clues for the origins of the stochasticity (e.g., Harrison and Giese 1988).

To illustrate the different developments of the two types of ENSO, Fig. 1 shows the lagged regression between observed EP/CP indices (definitions will be presented in Sect. 2.2.2) and the wind stress/SST anomalies. It can be clearly seen that the development of the EP type is very consistent with the canonical ENSO. Here, anomalous convection and its
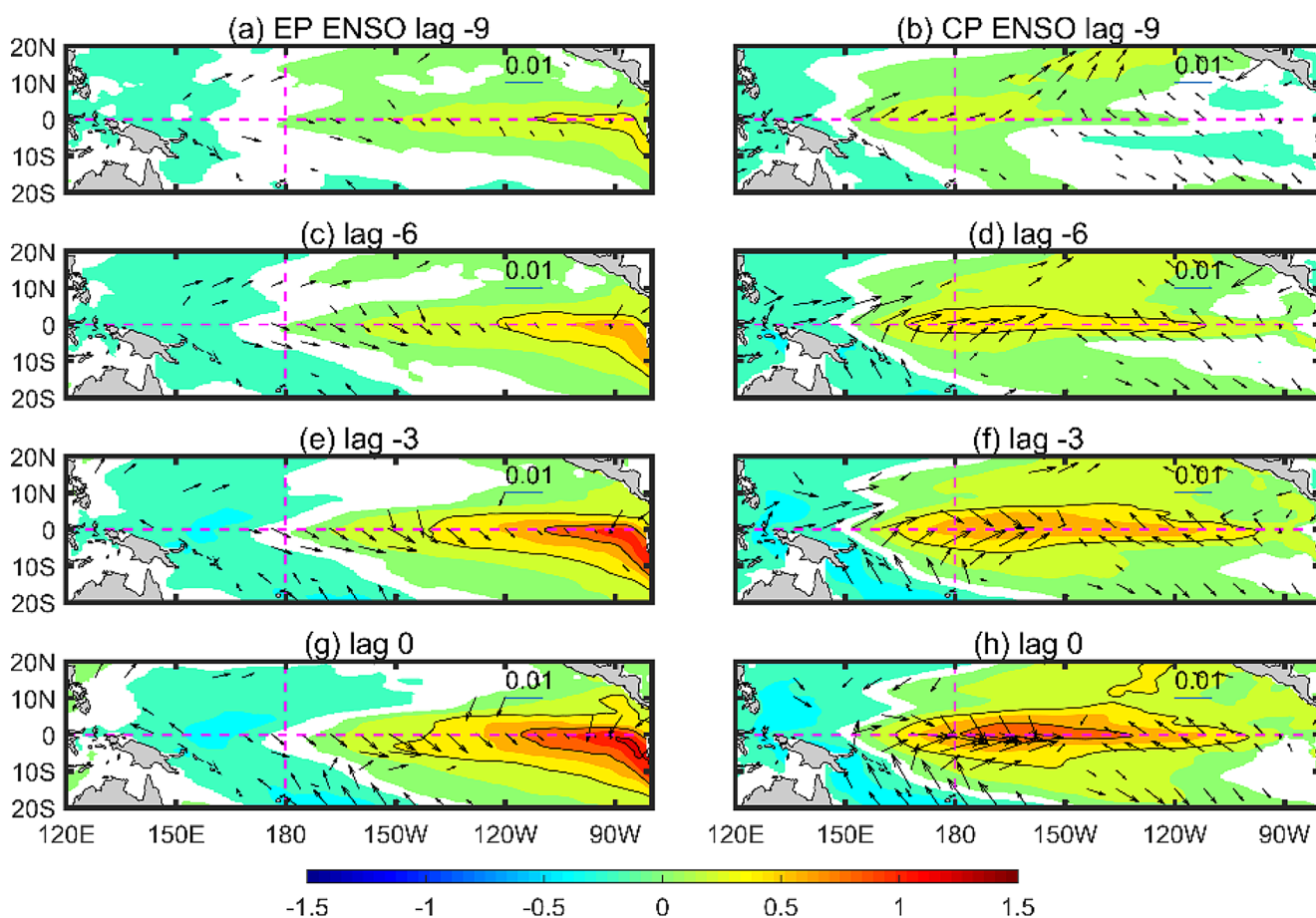

Fig. 1 Development of two types of ENSO events. Lagged regression coefficients between wind stress/SST anomalies in the tropical Pacific and EP/CP indices are in the left and right panels, respectively. Shading and contours are for the SST anomalies with the contour interval being 0.2 °C °C^{-1}. Arrows are for the wind stress anomalies. Values in the title of each panel indicate the months lagging the indices, namely, -9, -6, -3 and 0, and can be viewed as boreal spring, summer, autumn and winter of the ENSO developing year, respectively. Only coefficients exceeding the 95% confidence interval by a Student's t test are shown

related zonal wind stress are dominantly in the CP area, corresponding to the warming center located in the EP region. Different from the EP type, the main part of the relevant anomaly fields of the CP-type ENSO are located further westward. Especially at lag −9, that is, the boreal spring of the ENSO developing year, the main anomaly component is located west of the dateline. The significantly different spatial patterns determined by the lagged regression method is consistent with the typical development of two types of El Niño that can also be obtained through composite analysis (Kao and Yu 2009; Zheng et al. 2014; Fang and Mu 2018a). However, like classical ENSO theories, these studies only emphasized the importance of the zonal wind stress intensity and overlooked the impact of its position.

Physically, the Kelvin and Rossby waves excited by the westerly wind stress anomalies that are located more westward in spring are also closer to the WP coast. Because the Kelvin wave propagates so fast, the different longitudinal positions can hardly influence on the arrival of the downwelling signal to the EP region. On the contrary, different positions of the wind stress can impact the propagation period of the Rossby waves more significantly because their speed is much slower. This means that the interval between the originally excited downwelling and the reflected upwelling Kelvin waves by the WP coast becomes shorter with the westward movement of the westerly wind stress anomaly. For example, a 50°-longitude (∼5500 km along the equator) of westward movement of the westerly wind stress anomalies will delay the downwelling Kelvin wave for ∼25 days and the fastest upwelling Rossby waves for ∼75 days. Hence, there is a difference of 50 days for the growth of the SST anomalies (SSTa) in the EP region through the effective upwelling process and the large scale Bjerknes feedback. This provides a good opportunity for the SST in the CP region, which are more dominated by the zonal advective feedback, to be larger than those in the EP region, giving rise to a CP-type El Niño. As a result, the westward (eastward) movement of the westerly wind stress anomalies can be responsible for the westward (eastward) movement of the anomalous warming center. In this study, we will clarify this point using a linear regression model, and numerical simulations with the Zebiak-Cane (ZC) model (Zebiak and Cane 1987).

2 Data and methods

2.1 Data

The monthly mean SST and wind stress data used in this study are from the NCEP Global Ocean Data Assimilation System (GODAS) dataset (Behringer and Xue 2004). The

TCD is defined as the depth at which the oceanic potential temperature is 20 °C. The analysis period is from 1980 to 2020, and the interannual anomaly is obtained by removing the mean seasonal cycle after detrending of the whole period.

2.2 Methods

2.2.1 Zonal wind center index

To elucidate the importance of zonal wind position, an index of the wind center (or wind core) for the observational data is defined. There always exist both westerly and easterly anomalous winds along the equatorial central-western Pacific, i.e., the key area of 5° S–5° N, 120° E–160° W. It is the main component of the wind patch that dominates the driving effect on the underlying ocean, so its position is of major concern. The main component is the part of the zonal wind anomalies that have the same sign as the area averaged one. For example, if the averaged zonal wind anomalies in the equatorial central-western Pacific is positive, then the westerly anomalies in this area are treated as the main component, while the easterly anomalies are neglected. The zonal wind center is hence defined as the geometric center of the main-component zonal wind anomalies. Considering the importance of the wind direction, the zonal wind center is then specified with the sign of the main-component wind anomalies. Then, we get the zonal wind center index, which is termed as WC_W in this study.

2.2.2 EP and CP indices and selection of different ENSO events

To illustrate the differences between the two types of ENSO, the EP and CP indices are calculated based on the regression–empirical orthogonal function (EOF) method (Kao and Yu 2009). Specifically, the SSTa regressed on the Niño4 (5° S–5° N, 160° E–150° W) index are first subtracted from the original SSTa before the EOF analysis is conducted, and then the leading principal component is defined as the EP index to represent the EP ENSO variability. Similarly, the CP index is defined as the leading principal component of the SSTa in which the influence from the Niño1 + 2 (0°–10° S, 80°–90° W) index had been subtracted.

The method for clarifying the different ENSO events is the same as that employed by Fang et al. (2015). During the analysis period, five events are identified as CP El Niño: 1991/92, 1994/95, 2002/03, 2004/05, and 2009/10; eight events are identified as EP El Niño: 1982/83, 1986/87, 1987/88, 1997/98, 2006/07, 2014/15, 2015/16, and 2018/19; fourteen events are identified as La Niña: 1983/84, 1984/85,

1988/89, 1995/96, 1998/99, 1999/2000, 2000/01, 2007/08, 2008/09, 2010/11, 2011/12, 2016/17, 2017/18 and 2020/21.

2.2.3 Linear regression model

A simple linear regression model is next used to determine the importance of the zonal wind center on ENSO evolution. Guided by the classical theories, the mean zonal wind stress anomalies in the equatorial central-western Pacific (120° E–160° W, 5° S–5° N; termed as $\tau_a^x\_W$) and the basin mean TCDa along the equatorial Pacific (120° E–80° W, 5° S–5° N; termed as TCDa_M) are two crucial predictors for capturing the following ENSO development (Clarke and van Gorder 2001; Ren et al. 2019). Therefore, the binary linear regression model established by them is regarded as the reference. The importance of the zonal wind center is illustrated by a comparison between it and the ternary linear regression model that additionally includes WC_W. Considering the seasonal phase locking of ENSO (i.e., it always initiates in boreal spring, grows up to mature in winter, and quickly decays in the following spring), the relationship between the spring (March-May; MAM) predictors and ENSO indices at the end of the year (October–December; OND) is our main focus. So, the linear regression model used is,

$$
\begin{aligned}
Nino_p^{OND} =& a \times TCDa\_M_o^{MAM} \\
& + b \times \tau_a^x\_W_o^{MAM} + c \times WC\_W_o^{MAM} + d
\end{aligned}
\tag{1}
$$

where $Nino_p^{OND}$ is the OND mean Niño index and $TCDa\_M_o^{MAM}$, $\tau_a^x\_W_o^{MAM}$, and $WC\_W_o^{MAM}$ are the MAM mean TCDa_M, $\tau_a^x\_W$, and WC_W, respectively. The subscripts "p" and "o" are for the predicted and observed variables, respectively, and a, b, c, and d are the regression coefficients.

2.2.4 Sensitivity experiments with the ZC model

The classical ZC model is also used for sensitivity tests, which are designed as follows: two different zonal wind patches, whose shape and size are the same and the only difference is the position, are firstly adopted. The experiment of wind patch centering in the CP region (i.e., consistent with the classical ENSO theories) is called the EP experiment, while the experiment of wind patch centering in the WP region is called the CP experiment. Both experiments are cold start, that is, every variable is set to 0. The wind patch is imposed at the beginning of March and lasts for one month. Then, the wind patch is removed, and the experiment is continued for two years. The impact of the zonal wind center will be illustrated by comparing the results of these two experiments.

Like previous studies (Kug et al. 2003; An et al. 2008), the formulation of zonal wind patch is as follows,

$$
\tau_a^x(x,y) = A\exp\left(-\frac{(x-x_0)^2}{L_x^2} - \frac{y^2}{L_y^2}\right)
\tag{2}
$$

where x and y are the zonal and meridional directions, respectively, $L_x(32°)$ and $L_y(6°)$ are the zonal and meridional widths, respectively, while A is the amplitude, equal to a large value of 0.1 N m^{-2} in this study. Furthermore, x_0 is the center of the wind patch, which is 145.625° E and 195.625° E for the CP and EP experiments, respectively.

Then, more sensitivity experiments are conducted for further verify the importance of the zonal wind pattern on the following ENSO process and pattern. The results will be shown in Fig. 2.

3 Results

### 3.1 Zonal wind stress intensity vs. zonal wind stress center

To illustrate the possibly additional contribution of WC_W from $\tau_a^x\_W$ to the ENSO evolution, a comparison between these two indices is needed. For this purpose, Fig. 3 shows the scatter plot of WC_W and $\tau_a^x\_W$ for all the months and boreal spring. It can be seen that for both westerly and easterly wind stress situations, the linear relationships between these two indices are very weak, i.e., the correlation coefficients are small. This is more obvious for the situation during the spring season. So, this indicates that the zonal wind stress intensity is independent of the zonal wind stress center.

3.2 Linear regression model

Next, we explore the influence of the zonal wind position through the linear regression model introduced in Sect. 2, which is used to depict the connection between the spring precursors and the SSTa during the ENSO mature phase. The results are shown in Fig. 4. For comparison, the results of a binary regression model that uses only $\tau_a^x\_W$ and TCDa_M are also presented in Fig. 5.

It can be seen that the binary regression model based on the classical ENSO theory can well capture the variation of SST in the central-to-eastern Pacific. The correlation coefficients between the expected Niño3.4 and Niño3 indices by the model and the observations are 0.86 and 0.85, respectively, and the root mean square errors (RMSEs) are small as well, i.e., 0.34 °C and 0.4 °C. However, the model

Fig. 2 Winter (DJF mean) SSTa and τ_a^x along the equatorial Pacific to different positions of the zonal wind patch imposed in March. (**a**) shows the wind patches of different experiments, for which the patterns are the same as Fig. 2, but with different zonal positions. From left to right, the wind center linearly moves from 135.625° E to 195.625° E with a stride of 10°. (**b**) and (**c**) are for the DJF mean SSTa and τ_a^x accordingly. In each panel, the red and blue thick lines are for the two experiments illustrated in Fig. 2
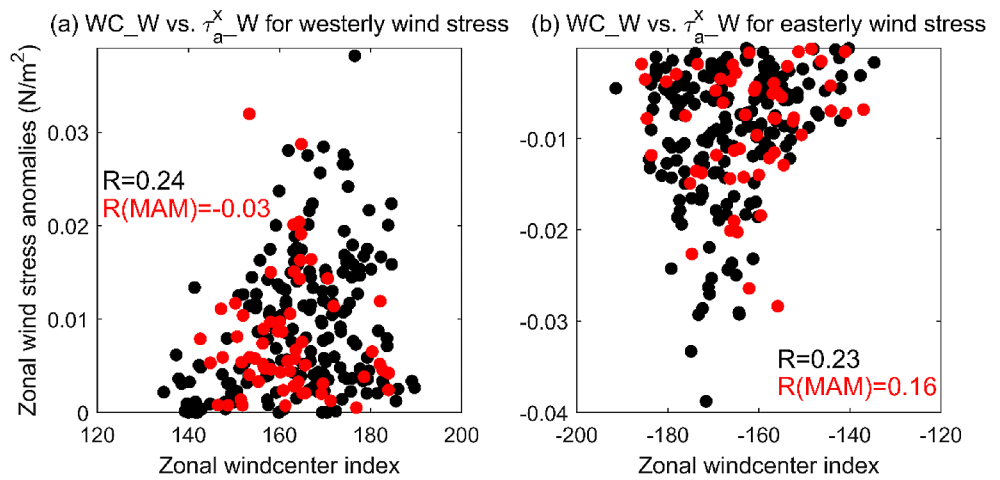
is insufficient to capture the Niño4 index (that represents SSTa relatively close to the CP region), for which the correlation coefficient drops to 0.79 and the adjusted R-square is 0.596, and the model significantly overestimates some EP El Niño events. In comparison, the model with WC_W index shows a significant improvement mainly for the Niño4 index. It shows that not only the correlation coefficient and adjusted R-square increase to a value that is comparable to the central-to-eastern Pacific (i.e., 0.84 and 0.675), but also the RMSE reduces to 0.2 °C. It should be noted that the improvements are more obvious for the CP El Niño and La Niña events. Calculation suggests that the correlation coefficients of Niño34, Niño3 and Niño4 indices for the binary regression model are respectively 0.84, 0.79 and 0.81 for these two types of ENSO events. While they are 0.89, 0.82 and 0.90 for the ternary regression one.

Comparing to the improvements on these two statistical merits, the more important indication from this analysis is the different physical interpretation. Specifically, it can be seen from the regression coefficients that the zonal wind center can be neglected for the SST development in the central-to-eastern Pacific, while the wind strength and warm water volume need to be kept (Fig. 4b and d), which is consistent with the classical ENSO theory. However, in the area closer to the CP, the center of the zonal wind stress is more important than its strength (Fig. 4f).

The dominant spatial pattern and the amplitude of the zonal wind center on the SST variations in the tropical Pacific are also determined. It can be seen from Fig. 6 that considering the WC_W index can make as large as 0.4 °C difference in standard deviation and 1.5 °C difference in range (i.e., the difference between the lowest and highest values) in the region near the date line, compared to the reference model. These results further suggest that a reasonable consideration of the zonal wind pattern and its influence on the oceanic dynamics is essential for representing

the SST variation in the CP area, and thus for capturing the diversity of ENSO.

3.3 ZC model experiment

By performing numerical simulations with the ZC model, we analyze the influence of different westerly wind positions at the initial state (March) on the subsequent air-sea coupling processes and the El Niño pattern. It can be seen from Fig. 7 that when the initial westerly wind stress is in the region east of the dateline, corresponding to the pattern of EP-type ENSO in Fig. 1, the excited downwelling Kelvin waves quickly propagate to the EP region (Fig. 7b) and then warm up the local SST through thermocline feedback. At the same time, the excited upwelling Rossby waves propagate westward at a much slower speed and are reflected as upwelling Kelvin waves after reaching the WP coast. The long interval between the downwelling and the reflected upwelling Kelvin waves provides ample time for SST growth in the EP region through the thermocline feedback. Therefore, the anomalous warming center is concentrated in the EP region (~123.75° W in this case), and an EP-type El Niño emerges during the mature phase with the well-established Sverdrup balance between the anomalous zonal wind stress and TCD gradient. As a comparison, when the initial westerly wind stress is in the region west of the dateline, corresponding to the pattern of CP-type ENSO in Fig. 1, the excited downwelling Kelvin waves also quickly propagate to the EP region and warm up the local SST. The Kelvin wave is so fast that there is only a slight difference in the SST variation during the first months between two experiments. However, in this situation, the upwelling Rossby waves can quickly travel to the WP coast and then be reflected as Kelvin waves, which significantly reduces the time for the growth of SST in the EP region through the thermocline feedback. This not only results in a smaller SSTa in the EP, which can be more clearly seen from the

Fig. 3 Relationship between the monthly zonal wind index (WC_W) and the zonal wind stress anomalies (τ_a^x_W) in the central-western Pacific during whole analysis period. Left and right panels are for the westerly and easterly wind stress component, respectively. Red dots are for the spring season (i.e., MAM). The correlation coefficients between these two indices for the total (black) and MAM (red) are also shown in the figure
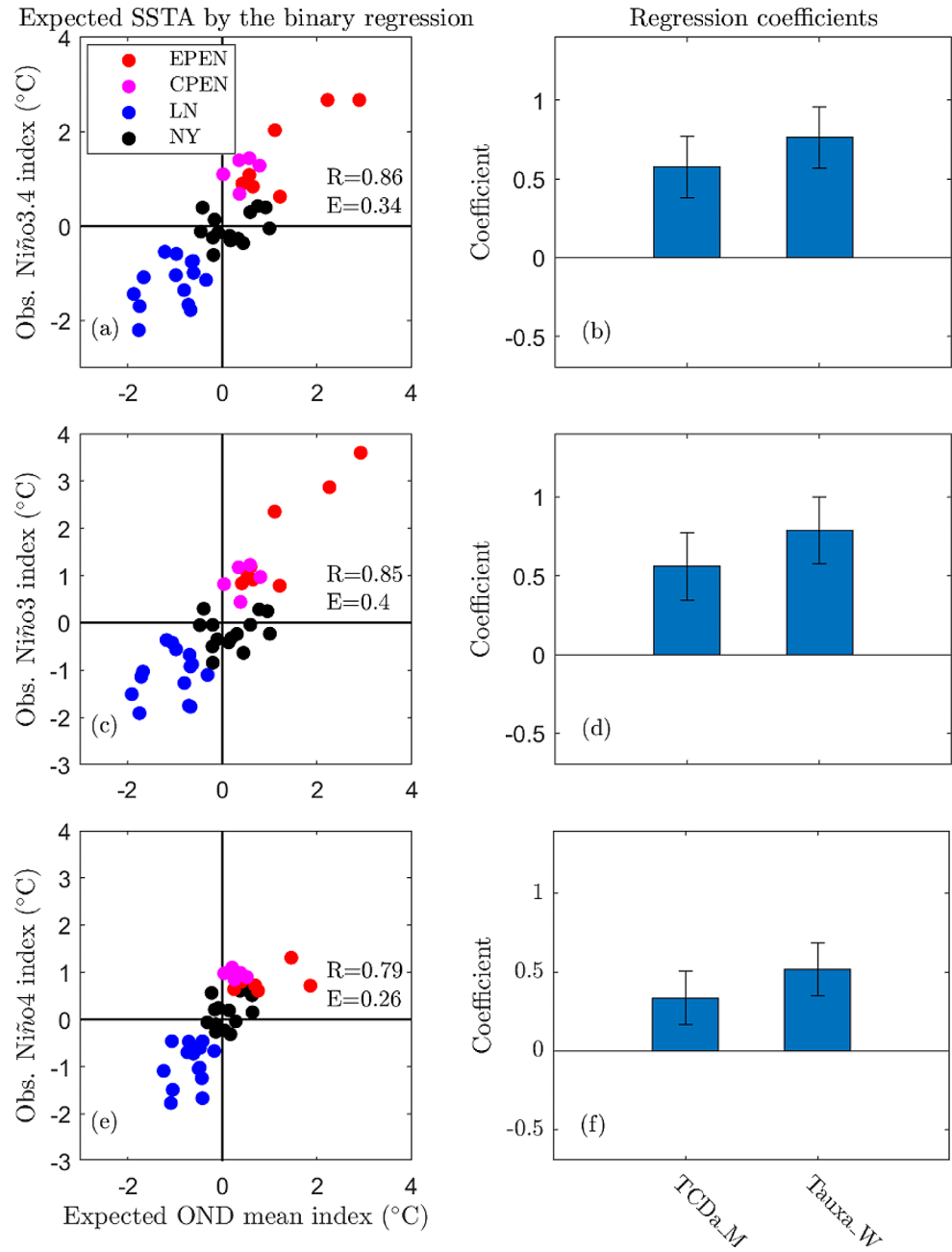
SSTa difference between the two experiments (Fig. 7d), but also makes its difference from those in the CP smaller, thus leading to the anomalous warming center to be more westward (~129.375° W in this case) like a CP-type El Niño. Correspondingly, the distributions of the anomalous TCD and zonal wind stress in subsequent evolution also move westward, compared with the EP experiment.

Except for these two representative examples, more sensitivity experiments with a different zonal wind center are further conducted with the ZC model. The results are presented in Fig. 2. It can be seen that with the westward movement of the zonal wind center in March, the centers

of the SSTa and τ_a^x (i.e., the position of the largest value of the variable) in the winter move westward consistently. More specifically, the center of the SSTa can move from almost ~110° W to ~140° W, with more than 30° longitude difference. Correspondingly, the center of τ_a^x can move from east of 150° W to ~170° W. Furthermore, with the warming center moving westward, the largest SSTa (or the El Niño amplitude) is also consistently decreasing, e.g., it is ~1 °C for the western-most situation while it can be larger than 4 °C for the eastern-most situation. These results suggest that the zonal wind center does have an important impact on the following ENSO process and pattern. Note

Fig. 4 Same as Fig. 6, but for the results from the ternary linear regression Eq. (1) using the MAM mean TCDa_M, τ_a^x_W, and WC_W indices
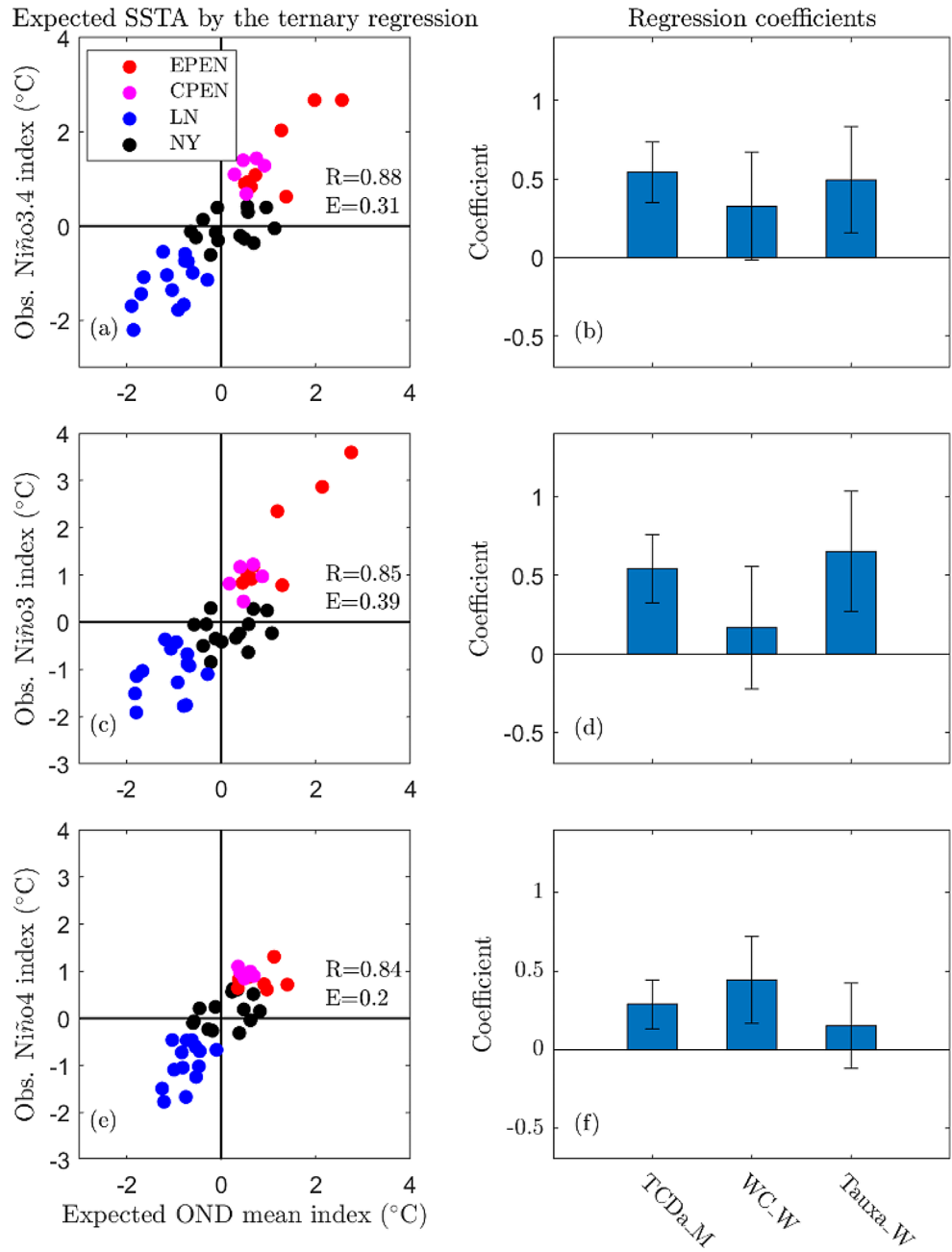
that the results from the experiments when the initial wind stress anomalies in MAM are imposed are consistent with the results here.

4 Conclusions and discussion

The diversity and complexity of ENSO has attracted extensive attention in recent years. Since the mean thermocline is shallow in the EP, the corresponding thermocline feedback is crucial to the SST variation. In the CP, the mean thermocline is relatively deep, so the role of the thermocline feedback is limited. However, the zonal SST gradient is strong here since the warm pool is to the west and cold tongue to the east. Therefore, the zonal advective feedback can effectively influence the local SSTa. Theoretical studies have confirmed this point (Kug et al. 2009; Fang and Mu 2018b), and some studies have constructed conceptual and intermediate complexity models that can simulate the complexity of ENSO by introducing stochastic processes (Chen et al. 2022; Chen and Fang 2023).

This paper emphasizes an overlooked aspect in deterministic ENSO theory, i.e. the importance of the spatial pattern of the zonal wind stress anomalies on ENSO type
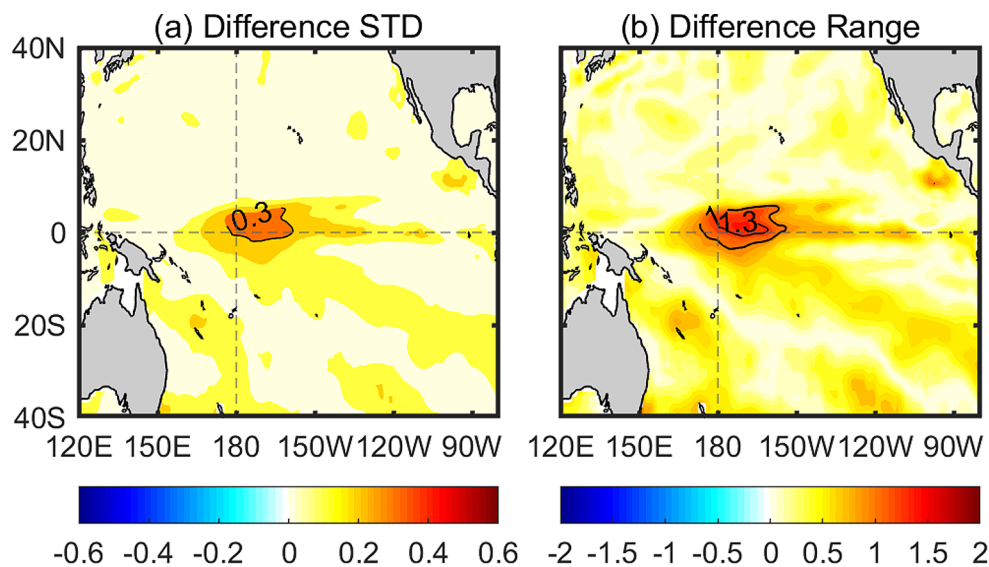
Fig. 5 Relations between the expected and observed Niño indices at the end of the year. The expected indices are obtained by the binary linear regression equation using the MAM mean TCDa_M and $\tau_a^{\tilde{x}}$ _W indices. (**a**), (**c**) and (**e**) are for the Niño3.4, Niño3 and Niño4 indices, respectively. The right panels show the corresponding coefficients (bars) and their 5% significance interval by Student's *t* test (error bars) of the two variables, which are obtained by the product of the regres-

sion coefficient of each variable and its corresponding standard deviation. The red, orange, blue dots in the left panels represent EP El Niño (EPEN), CP El Niño (EPEN) and La Niña (LN) events, respectively, whereas the black dots represent neutral years (NY). The correlation coefficient (R) and RMSE (E) between expected and observed Niño indices are also shown in the figure

and development. Specifically, if the westerly wind stress is closer to the WP, the excited upwelling Rossby waves will reach the WP coast and then be reflected as Kelvin waves in a shorter time. This significantly weakens SSTa in the EP region since less time is provided for the effective upwelling process and the large-scale thermocline feedback, which thus provides a good opportunity for the anomalous warming center to be closer to the CP region, i.e., the CP-type El Niño. This indicates that the location of zonal wind stress center has an important impact on the structure and strength of ENSO, and thus on its diversity and complexity.

Note that the SSTa pattern differences among different experiments are indeed much less than that observed between CP and EP El Niños. This mainly results from deficiencies of the ZC model. Actually, the ZC model was introduced during 1980s, when the ENSO diversity was not an issue and the main emphasis was to simulate and predict well the canonical EP type of ENSO. Since the primary process for the EP type of ENSO is the thermocline feedback, much less attention was put on the zonal advective feedback that is crucial for the SSTa variation on the equatorial central Pacific region. So, the strength of the zonal advective feedback is much underestimated in the original ZC model, which largely restricts the simulated SSTa amplitude in the CP region. Although we can very easily modify this by enlarge the zonal advective feedback strength in the CP region of the ZC model, the use of the original ZC model is preferred since its model components are well understood in

the ENSO community. The emphasis of these experiments is that with the westward movement of the westerly wind stress anomalies at its initial state, the warming SSTA center along the equatorial Pacific consistently moves westward, although there are still model biases preventing to capture a realistic SSTa pattern of different ENSO events.

Since boreal spring is the season with the weakest air-sea interaction in the tropical Pacific, the wind field can be more susceptible to other spatiotemporal processes, such as westerly wind bursts (WWBs), resulting in its complex characteristics. Observations show that WWBs mainly occur in the Indian Ocean (IO) and western-to-central Pacific regions. More specifically, the average numbers of WWBs per year over the IO, WP, and CP regions are 5.70, 3.88, and 3.18, respectively (Lian et al. 2018). Hence, stochastic aspects of the WWB occurrence in both WP and CP regions can affect the spatial pattern of the zonal wind-stress anomalies on the interannual scale. In addition, also extratropical physical processes can affect the wind-stress field in the equatorial Pacific (Ham et al. 2019; Cai et al. 2019; Wang et al. 2022). Hence, further clarifications on the sources of different wind stress anomaly patterns in spring is of great significance for simulating and predicting the type of ENSO.

Fig. 6 Differences in SST variation induced by zonal wind position. (**a**) and (**b**) show the differences in the standard deviation (STD; °C) and range (°C) of the ternary linear regression model induced SST variation from those of the binary model that only depends on the TCDa_M and τ_a^x_W indices, respectively
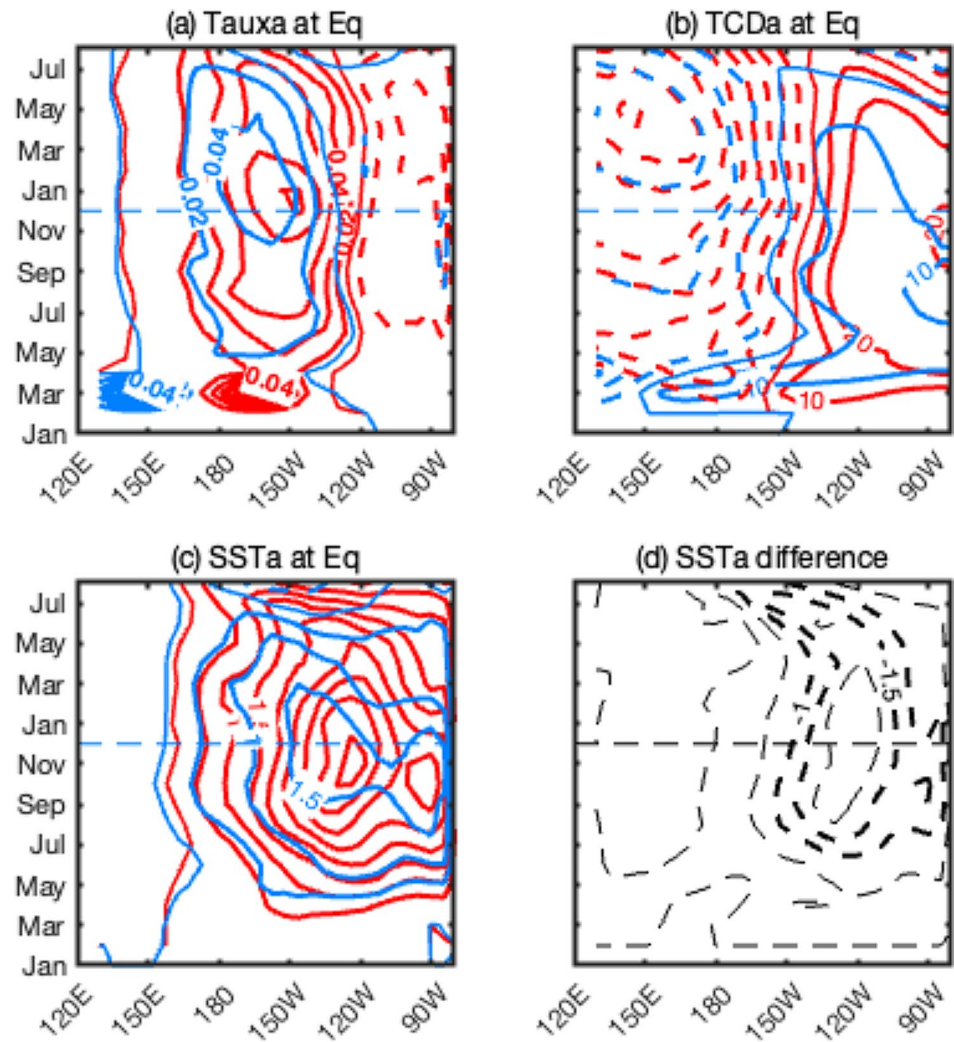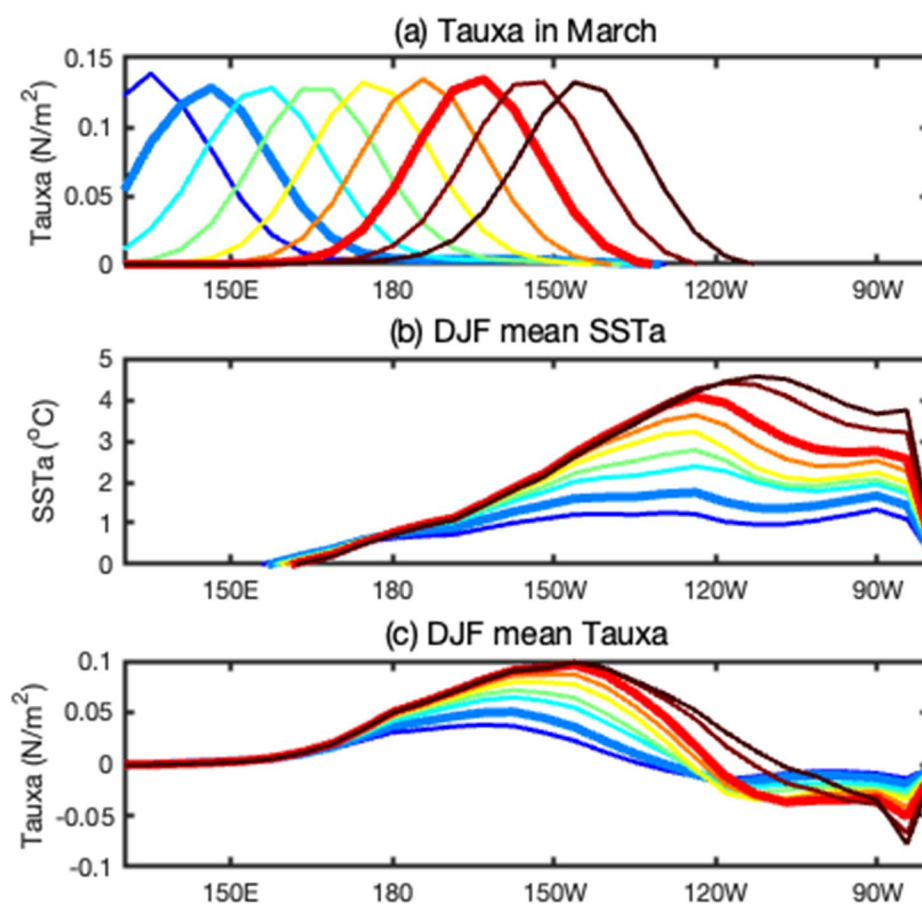
Fig. 7 Air-sea evolution in the equatorial Pacific responded to different positions of the zonal wind patch. For each experiment, the wind patch is imposed in March. The blue and red contours are for the CP and EP experiments, respectively. (**a**), (**b**) and (**c**) are for the 5° S–5° N averaged zonal wind stress anomalies (N m^{-2}; contour interval is 0.02), TCDa (m; contour interval is 10), and SSTa (°C; contour interval is 0.5), respectively. (**d**) shows the SSTa difference between the two experiments, i.e., the result of CP experiment minuses that of EP experiment

Data availability The GODAS reanalysis is obtained at https://www.psl.noaa.gov//data/gridded/data.godas.html, the GPCP data is at https://psl.noaa.gov/data/gridded/data.gpcp.html.

Declarations

Competing interests The authors declare no competing interests

References

An S-I, Kug J-S, Ham Y-G et al (2008) Successive modulation of ENSO to the future greenhouse warming. J Clim 21(1):3–21. https://doi.org/10.1175/2007JCLI1500.1

Battisti DS (1988) Dynamics and thermodynamics of a warming event in a coupled tropical atmosphere–ocean model. J Atmos Sci 45(20):2889–2919. https://doi.org/10.1175/1520-0469(1988)045%3C2889:DATOAW%3E2.0.CO;2

Behringer D, Xue Y (2004) Evaluation of the global ocean data assimilation system at NCEP: The Pacific Ocean. Proceedings eighth symposium on integrated observing and assimilation systems for atmosphere, oceans, and land surface [Dataset]. Retrieved from https://www.researchgate.net/publication/2288

Bjerknes J (1969) Atmospheric teleconnections from the equatorial Pacific. Mon Weather Rev 97(3):163–172. https://doi.org/10.1175/1520-0493(1969)097%3C0163:ATFTEP%3E2.3.CO;2

Cai W-J et al (2019) Pantropical climate interactions. Science 363:944. https://doi.org/10.1126/science.aav4236

Capotondi A et al (2015) Understanding ENSO diversity. Bull Am Meteorological Soc 96:921–938. https://doi.org/10.1175/BAMS-D-13-00117.1

Chen N, Fang X (2023) A simple Multiscale Intermediate coupled Stochastic Model for El Niño Diversity and Complexity. J Adv Model Earth Syst 15(4). https://doi.org/10.1029/2022MS003469

Chen N, Fang X, Yu J-Y (2022) A multiscale model for El Niño complexity. Npj Clim Atmospheric Sci 5:16. https://doi.org/10.1038/s41612-022-00241-x

Clarke AJ, van Gorder S (2001) ENSO prediction using an ENSO trigger and a proxy for western equatorial pacific warm Pool Movement. Geophys Res Lett 28(4):579–582. https://doi.org/10.1029/2000GL012201

Fang X, Chen N (2023) Quantifying the predictability of ENSO complexity using a statistically accurate multiscale stochastic model and information theory. J Clim 36(8):2681–2702. https://doi.org/10.1175/JCLI-D-22-0151.1

Fang X, Mu M (2018a) Both air-sea components are crucial for El Niño forecast from boreal spring. Sci Rep 8(1):1–8. https://doi.org/10.1038/s41598-018-28964-z

Fang X, Mu M (2018b) A three-region conceptual model for central Pacific El Niño including zonal advective feedback. J Clim 31:4965–4979. https://doi.org/10.1175/JCLI-D-17-0633.1

Fang X, Zheng F (2021) Effect of the air-sea coupled system change on the ENSO evolution from boreal spring. Clim Dyn 57:109–120. https://doi.org/10.1007/s00382-021-05697-w

Fang X, Zheng F, Zhu J (2015) The cloud-radiative effect when simulating strength asymmetry in two types of El Niño events using CMIP5 models. J Geophys Research: Oceans 120(6):4357–4369. https://doi.org/10.1002/2014JC010683

Fang X, Dijkstra H, Wieners C, Guardamagna F (2024) A nonlinear full-field conceptual model for ENSO diversity. J Clim. https://doi.org/10.1175/JCLI-D-23-0382.1

Geng L, Jin F-F (2022) ENSO diversity simulated in a revised Cane-Zebiak model. Front Earth Sci 10:899323. https://doi.org/10.3389/feart.2022.899323

Geng L, Jin F-F (2023) Insights into ENSO Diversity from an intermediate coupled model. Part II: role of Nonlinear Dynamics and Stochastic forcing. J Clim 36:7527–7547. https://doi.org/10.1175/JCLI-D-23-0044.1

Geng T, Cai W, Wu L (2020) Two types of ENSO varying in tandem facilitated by nonlinear atmospheric convection. Geophys Res Lett 47(15). https://doi.org/10.1029/2020GL088784

Ham Y-G, Kim J-H, Luo J-J (2019) Deep learning for multi-year ENSO forecasts. Nature 573:568–572. https://doi.org/10.1038/s41586-019-1559-7

Harrison DE, Giese BS (1988) Remote westerly wind forcing of the eastern equatorial Pacific; some model results. Geophys Res Lett 15(8):804–807. https://doi.org/10.1029/GL015i008p00804

Jin F-F (1997) An equatorial ocean recharge paradigm for ENSO. Part I: conceptual model. J Atmos Sci 54(7):811–829. https://doi.org/10.1175/1520-0469(1997)054%3C0811:AEORPF%3E2.0.CO;2

Kao H-Y, Yu J-Y (2009) Contrasting eastern-pacific and central-pacific types of ENSO. J Clim 22(3):615–632. https://doi.org/10.1175/2008JCLI2309.1

Klein SA, Soden BJ, Lau N-C (1999) Remote sea surface temperature variations during ENSO: evidence for a tropical atmospheric bridge. J Clim 12:917–932. https://doi.org/10.1175/1520-0442(1999)012%3C0917:RSSTVD%3E2.0.CO;2

Kug I-S, Kang I-S, An S-I (2003) Symmetric and antisymmetric mass exchanges between the equatorial and off-equatorial Pacific associated with ENSO. J Geophys Research: Oceans 108(C8). https://doi.org/10.1029/2002JC001671

Kug JS, Jin F-F, An SI (2009) Two types of El Niño events: Cold tongue El Niño and warm pool El Niño. J Clim 22(6):1499–1515. https://doi.org/10.1175/2008JCLI2624.1

Lian T, Tang Y, Zhou L et al (2018) Westerly wind bursts simulated in CAM4 and CCSM4. Clim Dyn 50:1353–1371. https://doi.org/10.1007/s00382-017-3689-7

McPhaden MJ (2003) Tropical Pacific Ocean heat content variations and ENSO persistence barriers. Geophys Res Lett 30(9). https://doi.org/10.1029/2003GL016872

McPhaden MJ, Zebiak SE, Glantz MH (2006) ENSO as an integrating concept in Earth science. Science 314:1740–1745. https://doi.org/10.1126/science.1132588

Meinen CS, McPhaden MJ (2000) Observations of warm water volume changes in the equatorial Pacific and their relationship to El Niño and La Niña. J Clim 13(20):3551–3559. https://doi.org/10.1175/1520-0442(2000)013%3C3551:OOWWVC%3E2.0.CO;2

Pang D, Fang X, Wang L (2023) Importance of realistic zonal currents in depicting the evolution of tropical central Pacific sea surface temperature. Environ Res Lett 18(12):124031. https://doi.org/10.1088/1748-9326/ad0b21

Philander S (1983) El Niño Southern Oscillation phenomena. Nature 302(5906):295–301. https://doi.org/10.1038/302295a0

Ren HL, Zuo J, Deng Y (2019) Statistical predictability of Niño indices for two types of ENSO. Clim Dyn 52:5361–5382. https://doi.org/10.1007/s00382-018-4453-3

Ropelewski CF, Halpert MS (1987) Global and regional scale precipitation patterns associated with the El Niño/Southern Oscillation. Mon Weather Rev 115:1606–1626. https://doi.org/10.1175/1520-0493(1987)115%3C1606:GARSPP%3E2.0.CO;2

Ruiz JE, Cordery I, Sharma A (2005) Integrating ocean subsurface temperatures in statistical ENSO forecasts. J Clim 18(17):3571–3586. https://doi.org/10.1175/JCLI3477.1

Schopf PS, Suarez MJ (1988) Vacillations in a coupled ocean–atmosphere model. J Atmos Sci 45:549–566. https://doi.org/10.1175/1520-0469(1988)045%3C0549:VIACOM%3E2.0.CO;2

Tang Y et al (2018) Progress in ENSO prediction and predictability study. Natl Sci Rev 5:826–839. https://doi.org/10.1093/nsr/nwy105

Timmermann A et al (2018) El Niño–Southern Oscillation complexity. Nature 559:535–545. https://doi.org/10.1038/s41586-018-0252-6

Wang C (2018) A review of ENSO theories. Natl Sci Rev 5(6):813–825. https://doi.org/10.1093/nsr/nwy104

Wang J, Zhang S, Jiang H, Yuan D (2022) Effects of 2019 subsurface Indian Ocean initialization on the forecast of the 2020/2021 La Niña event. Clim Dyn 1–17. https://doi.org/10.1007/s00382-022-06442-7

Zebiak SE, Cane MA (1987) A model El Niño–Southern Oscillation. Mon Weather Rev 115(10):2262–2278. https://doi.org/10.1175/1520-0493(1987)115%3C2262:ameno%3E2.0.co;2

Zhang R, Min Q, Su J (2017) Impact of El Niño on atmospheric circulations over East Asia and rainfall in China: role of the anomalous western North Pacific anticyclone. Sci China Earth Sci 60:1124–1132. https://doi.org/10.1007/s11430-016-9026-x

Zheng F, Fang X, Yu J-Y, Zhu J (2014) Asymmetry of the bjerknes positive feedback between the two types of El Niño. Geophys Res Lett 41(21):7651–7657. https://doi.org/10.1002/2014GL062125